



## Novel molecularly imprinted polymer prepared by palygorskite as support for selective adsorption of bisphenol A in aqueous solution

Zilong Zhao<sup>a</sup>, Dafang Fu<sup>a,\*</sup>, Binsheng Zhang<sup>a,b</sup>

<sup>a</sup>Department of Municipal Engineering, Southeast University, Nanjing 210096, China, emails: [berthillon@hotmail.com](mailto:berthillon@hotmail.com) (Z. Zhao), [fd@seu.edu.cn](mailto:fd@seu.edu.cn) (D. Fu), [seuzbs@hotmail.com](mailto:seuzbs@hotmail.com) (B. Zhang)

<sup>b</sup>School of Civil and Environmental Engineering, Harbin Institute of Technology Shenzhen Graduate School, Shenzhen 518055, China

Received 2 October 2014; Accepted 9 May 2015

### ABSTRACT

Novel strategy to synthesize palygorskite-supported surface molecularly imprinted polymer (SMIP) for bisphenol A (BPA) template was presented. Fourier transform infrared, scanning electron microscopy, and elemental analysis were employed for the characterization of the resulting composites. When compared with the molecularly imprinted polymer, the SMIP exhibited more excellent affinity and selectivity towards BPA in aqueous solution, with the affinity constant ( $b$ ) of 1.929, the Freundlich constants ( $K_F$ ) of 25.758, and the distribution coefficient ( $K_d$ ) of 128.390. The adsorption behaviors of the SMIP were well described by Freundlich isotherm model and the pseudo-second-order model. Moreover, the sustainable reusability of the SMIP without significant loss in rebinding capacity was affirmed in four repeated cycles. These results demonstrated the potential of the prepared SMIP as an advanced separation materials for the elimination of specific endocrine disruptor in aquatic environment.

*Keywords:* Surface molecularly imprinted polymer; Palygorskite; BPA

### 1. Introduction

Bisphenol A (BPA), as an essential organic chemical, has been widely reported to occur in miscellaneous environmental matrices, including air, indoor dust, aquatic systems, soil, sediment, sewage sludge, foodstuffs, paper products, as well as human colostrum, blood, and urine [1–7]. With the revelation of its acute reproductive toxicity, suspected carcinogenicity and mutagenicity [7], BPA has been identified as one of endocrine disrupting compounds (EDCs) and the acceptable daily inhalation dose for the general

population is presumed to be lower than  $0.003 \mu\text{g kg}^{-1} \text{bw day}^{-1}$  in the case of the contribution of non-dietary sources [5]. Since the inherently hydrophobic of most EDCs, the operation of their removal by physical adsorption methods are recommended actively by U.S. Environmental Protection Agency (USEPA) and National Primary Drinking Water Regulations [8]. However, the use of traditional activated carbon, for the separation of EDCs at trace concentration, can be adversely affected by concentration gradients and competing organic pollutants, making it an unreliable treatment option. Great attention has been focused on the development of advanced adsorbent materials with high performance for the EDCs treatment. For

\*Corresponding author.

example, carbon nanomaterials including graphene, single-walled carbon nanotube, and multi-walled carbon nanotube were reported for separation of bisphenol AF, BPA, and 17 $\alpha$ -ethinyl estradiol (EE2) [9,10]. Surface-modified mesoporous silica resulted in an effective removal of nonylphenol in the presence of phenol [11]. Novel functional polypropylene, prepared by the grafting of hydrophilic and hydrophobic monomer, was studied for removing different EDCs from aqueous solution, such as BPA, dibutyl phthalate, dimethyl phthalate, and dioctyl phthalate [12]. In addition, molecularly imprinted polymer (MIP) has also been utilized as separation media and support affinity for estrogen removal purposes [8,13].

Based on biological theory of antigen–antibody interactions, molecular imprinting is inherently an efficient technique of synthesizing “tailor-made” recognition sites and cavities in the macromolecule polymerization systems, which are complementary to the shape, size, and functionality of the template. The resulting polymer matrixes have been conceived to be highly specific targeting and sensitive and can concentrate the target molecular even under the presence of its structural analogs. Compared with the conventional bulk polymerization method, surface molecular imprinting explored by generating binding sites on the surface of some matrix materials, was more favorable to increase accessible sites, improve the binding rate between the template molecules and recognition sites, and design the predetermined imprinted polymers for macromolecules template [14]. Many particles, such as chitosan–Fe<sub>3</sub>O<sub>4</sub> nanoparticles [15], carbon microspheres [16], silica microparticles [17,18], porous alumina membrane [19], and quantum dots [20] have already been reported as reliable supporting matrices in the surface imprinting process.

Palygorskite is a kind of hydrated magnesium aluminum silicate mineral with fibrous rod-like microstructure. Owing to its excellent structural properties and physicochemical characters (e.g. high surface area, chemical stability, moderate cation exchange capacity and plentiful activated silanol groups), palygorskites have great potential as inexpensive and efficient adsorbents and carriers for current sewage purification [21,22]. To the best of our knowledge, so far rare research regards the study of natural clay as a support matrix for surface molecularly imprinted polymer (SMIP), especially palygorskite. In this research, a novel imprinted polymer on the surface of palygorskite using BPA as the template molecule was first synthesized by precipitation polymerization method. The structural characteristics, adsorption behaviors, and the regeneration ability of the resulting polymers were investigated and discussed in detail.

## 2. Experimental

### 2.1. Materials

Natural palygorskite clay, supplied by Golden Stone Palygorskite Research and Development Center (Jiangsu, China) was manually ground and sieved through a 100-mesh (150 micron) screen. Glycidoxypropyltrimethoxysilane (KH-560) (Sinopharm Chemical Reagent Co., Ltd. China) was selected as the surface-treating agent for palygorskite. The functional monomer of 4-vinyl pyridine (4-VP), the cross-linker of trimethylolpropane trimethacrylate (TRIM), and the initiator, azobisisobutyronitrile (AIBN) were supplied from Aladdin-reagent Inc. (Shanghai, China). Prior to use, TRIM and 4-VP were purified to remove the polymerization inhibitor and AIBN was recrystallized from methanol and then dried at room temperature. Acetonitrile, used as a reaction solvent in the polymerization reaction, was purchased from Sinopharm Chemical Reagent Co., Ltd. China. BPA and its structural analogs, *p*-tert-butylphenol (4-TBP), and hydroquinone (HQ), supplied by Guangfu Fine Chemical Research Institute (Tianjin, China), were used as competitive target compounds to be removed in this study. The individual stock standard solutions of the target compounds were prepared by dissolving 1 g of the target compound in 1,000 mL distilled water. Working standard solutions were prepared by appropriate dilution of the stock standard solutions. Other reagents used were all of analytical grade and distilled water was employed throughout the experiments.

### 2.2. Preparation of SMIP

Acid-activated palygorskite was prepared as described by Frini-Srasra and Srasra [23]. Then, acid-treated palygorskite (10 g) was dispersed in 200 mL distilled water and conditioned to pH 4–6 with hydrochloric acid. Afterward, KH-560 (2 g) was added into above solution. The mixture was stirred at 80°C for 5 h. Finally, the silylated palygorskite was filtered, washed, and dried before screening.

In the next step, silylated palygorskite (10 g) was added to 100 mL of 0.05 mol L<sup>-1</sup> HCl by refluxing at 50°C for 3 h under nitrogen atmosphere, then filtered, washed, and dried. The resulting palygorskite (2 g) was transferred to 40 mL toluene and followed by the addition of 2 mL acryloyl chloride and 3.5 mL triethylamine in a nitrogen atmosphere. The reaction was initiated at room temperature and maintained for 24 h under magnetic stirring. Next, the product were washed with toluene, acetone, ether, and methanol repeatedly and dried at 50°C, yielding the desired modified palygorskite.

The preparation of SMIP at surface of the modified palygorskite was as follows. BPA (0.1 mmol), 4-VP (0.4 mmol) and modified palygorskite (500 mg) were added into 25 mL acetonitrile. The mixture was magnetically stirred for 2 h, and degassed by sonication for 20 min. To this were added TRIM (2 mmol) and AIBN (30 mg) successively. The above mixed solution was then purged with nitrogen for 5 min and stirred at 60°C for 24 h. The final products were treated with formic acid–acetic acid (9:1, v/v) and ethanol repeatedly, and then dried at 50°C. For comparison, MIP was prepared under the same procedure only without adding palygorskite.

### 2.3. Characterization

The morphologies of all samples were examined using S-3400 N II (Hitachi) scanning electron microscopy (SEM). Fourier transform infrared (FT-IR) spectra (4,000–400  $\text{cm}^{-1}$ ) using KBr were recorded on a NEXUS870 (Nicolet) spectrometer. The carbon and hydrogen contents were determined by a CHN–O–Rapid (Heraeus) elemental analyzer.

### 2.4. Adsorption experiments

For the adsorption kinetics experiments, 5 mg SMIP or MIP was dispersed in 6 mL BPA solution with an initial concentration of 20  $\text{mg L}^{-1}$  and shaken continuously at 298 K for measuring the adsorption capacity as a function of time. For the adsorption isotherms experiments, 5 mg SMIP or MIP was equilibrated with 6 mL BPA solutions of different concentrations at 298 and 308 K, respectively, and the concentration of BPA in the supernatant was determined by UV spectrophotometer at 278 nm. The adsorption amount and removal efficiency of BPA adsorbed by SMIP or MIP were calculated according to the following equation:

$$Q_e = \frac{(C_0 - C_e)V}{W} \quad (1)$$

$$\text{Removal efficiency (\%)} = \frac{(C_0 - C_e)}{C_0} \times 100\% \quad (2)$$

where,  $Q_e$  ( $\text{mg g}^{-1}$ ) is the adsorption amount at equilibrium;  $C_0$  and  $C_e$  ( $\text{mg L}^{-1}$ ) are the initial and equilibrium concentrations of BPA, respectively;  $V$  (mL) is the volume of the BPA solution and  $W$  (mg) is the mass of the adsorbent.

To measure the selective recognition for BPA, 5 mg SMIP or MIP were added into 6 mL mixed solutions

containing 5  $\text{mg L}^{-1}$  of BPA, 4-TBP, and HQ. After shaking for 2 h at 298 K, the concentrations of BPA, 4-TBP, and HQ were determined by HPLC at the conditions given below: the mobile phase consisted of 60% acetonitrile and 40% distilled water, at a flow rate of 1.0  $\text{mL min}^{-1}$ , and the injection volume was 20  $\mu\text{L}$ . The recognition selectivity was evaluated by the distribution coefficient ( $K_d$ ,  $\text{L g}^{-1}$ ) and selectivity coefficient ( $k$ ) which were defined as follows:

$$K_d = \frac{Q_c}{C_c} \quad (3)$$

$$k = K_d[\text{BPA}]/K_d[M] \quad (4)$$

where  $K_d[\text{BPA}]$  and  $K_d[M]$  represent the distribution coefficients of BPA and the one of the other competitive target compounds, respectively.

### 2.5. Regeneration and reuse

Upon equilibrium, the SMIP loaded with BPA was ultrasonically eluted by the mixed solvent of methanol/acetic (9:1, v/v) and then washed with methanol. The regenerated SMIP was reused for the subsequent adsorption, and the consecutive adsorption/desorption cycles were repeated under the same conditions four times as adsorption experiments.

## 3. Results and discussion

### 3.1. Preparation and characterization

The SMIP preparation procedure is illustrated in Fig. 1, which includes acid-activation, silylation, ring opening, acylation, and precipitation polymerization. Compared to the natural palygorskite, acid activation may be endowed with additional Si–OH groups, allowing the formation of a more stable unite by reacting with the alkoxy groups at one end of silane coupling agent. For improving the surface activity of as-prepared silylated palygorskite, a great amount of double bonds were introduced onto the surface of silylated palygorskite by ring opening and acylation. Meanwhile, in the presence of the initiator, these double bonds could be readily grafted to polymerization system by addition reactions, leading to the spontaneous deposition of MIP around the surface of the modified palygorskite. The BPA imprinted material was eventually obtained after the removal of the embedded template molecule.

The typical SEM examination (Fig. 2) revealed that purified palygorskite displayed short rod-shaped

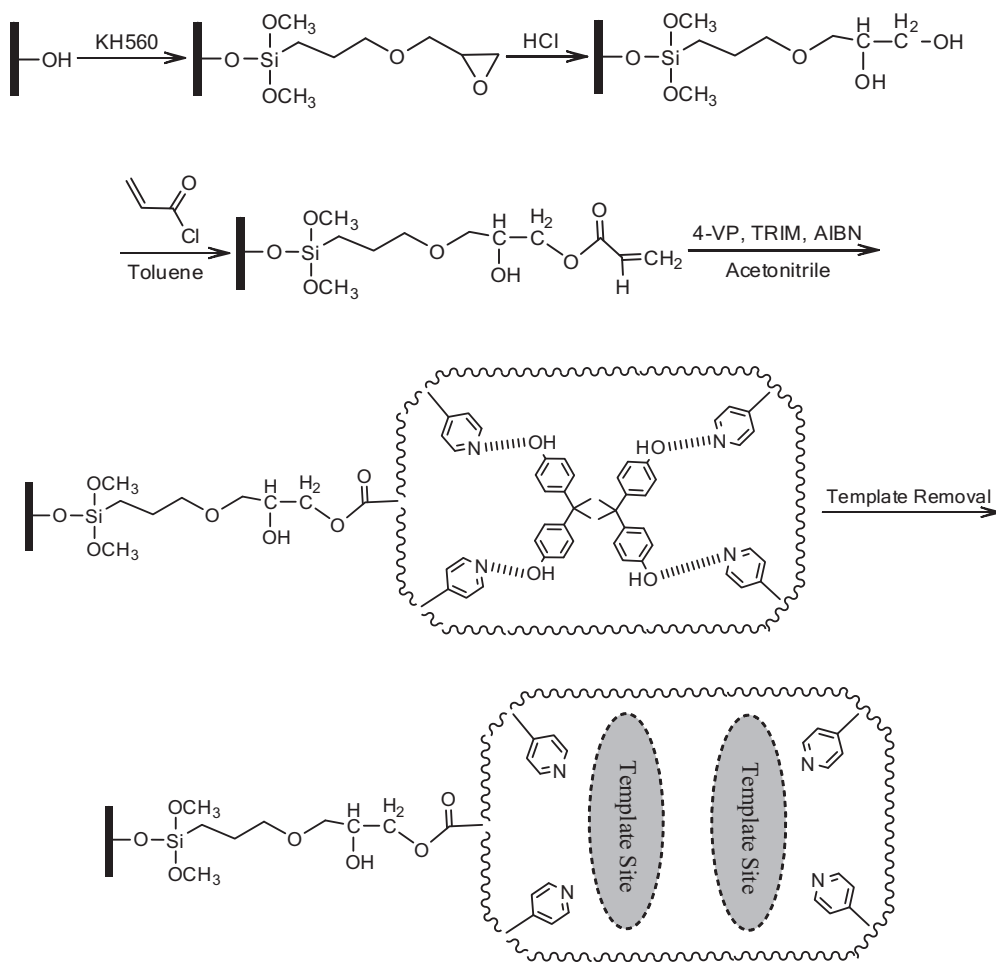


Fig. 1. Preparation of SMIP.

form, and many rods intricately accumulated and presented random orientation in some circular aggregation. Morphologic differences between purified palygorskite and silylated palygorskite are not significant, but more isolated rod particles were observed noticeably, probably due to the reduction of the interactions between palygorskite single crystals in the presence of the silane coupling agent. After being grafted with MIP, the surface morphology of palygorskite appeared as a smoother ellipse, with larger size distributions ranging from 3 to 6  $\mu\text{m}$ , which suggested that thin imprinted polymer was formed from the solution polymerization at the surface of palygorskite, and not from the physical adsorption to the polymer formed in solution phase.

To further confirm the formation of imprint polymer layer on the surface of palygorskite, FT-IR spectra and elemental analysis were conducted to characterize purified palygorskite, silylated palygorskite, and SMIP (Fig. 3). Specifically, in the case of purified

palygorskite, the bands at 3,615, 3,583, and 3,552  $\text{cm}^{-1}$  are attributed to  $\nu(\text{Mg, Al})\text{OH}$ ,  $\nu\text{Mg}_2\text{OH}$ , and  $\nu(\text{Fe}^{3+}, \text{Mg})\text{OH}$ , respectively. The band centered at 1,658  $\text{cm}^{-1}$  corresponds to  $\text{OH}_2$  bending vibration. Several bands observed in the area of 1,200–900  $\text{cm}^{-1}$  originate from Si–O–Si and Si–O symmetric or asymmetric stretching vibrations [24], and the bands at around 476  $\text{cm}^{-1}$  are assigned to the bending vibrations of Si–O framework [25]. After the assembly of silane-coupling agent onto the surface of palygorskite, the additional peaks, assigned to C–H stretching bands of both  $\text{CH}_3$  and  $\text{CH}_2$  groups, were found at 2,929 and 2,855  $\text{cm}^{-1}$ , despite the weak adsorption intensity. It can be inferred that palygorskite, with less inherent silanol groups at the external edge and basal surfaces, may go against the occurrence of the silylation.

From Fig. 3, it can be observed that the FT-IR spectra of SMIP showed many variations from that of the sample after grafting imprint polymer. Among the characteristic bands of the SMIP, those at 1,738  $\text{cm}^{-1}$

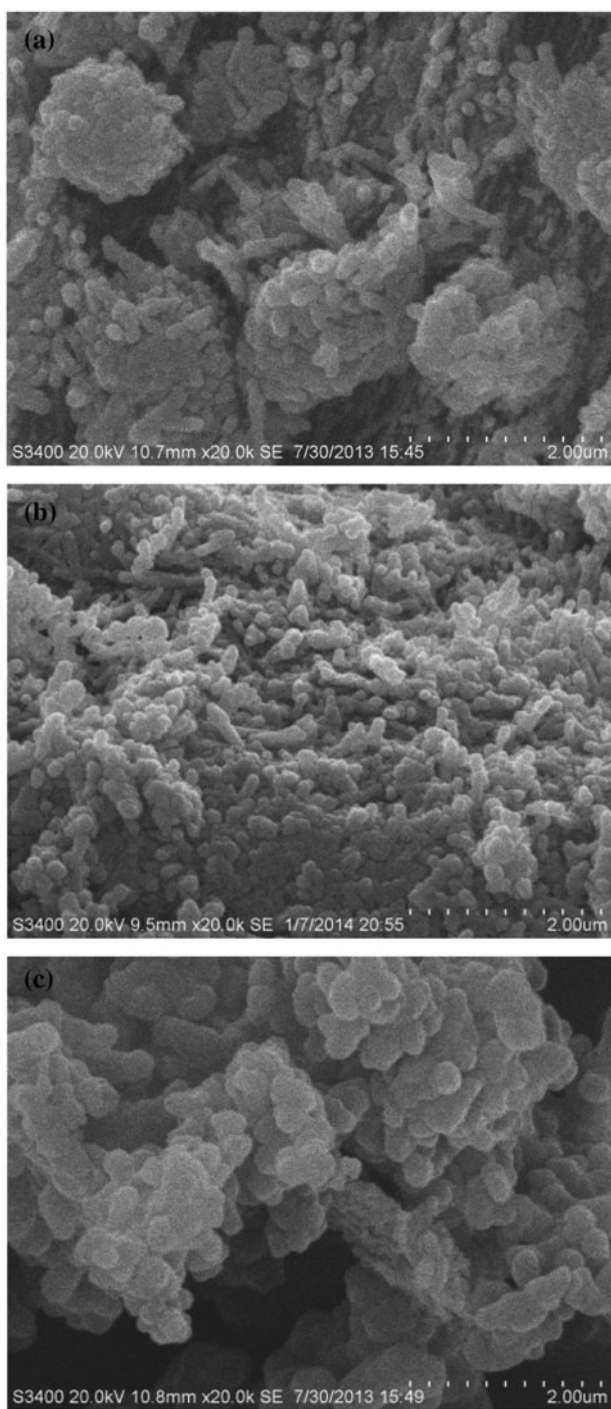


Fig. 2. SEM micrograph of (a) purified palygorskite, (b) silylated palygorskite, and (c) SMIP.

may correspond to C=O stretching vibration of carbonyl groups, indicating the existence of addition reaction between double bonds in the modified palygorskite and the cross-linker, while those in the range of 1,600–1,390  $\text{cm}^{-1}$  are attributed to the stretching

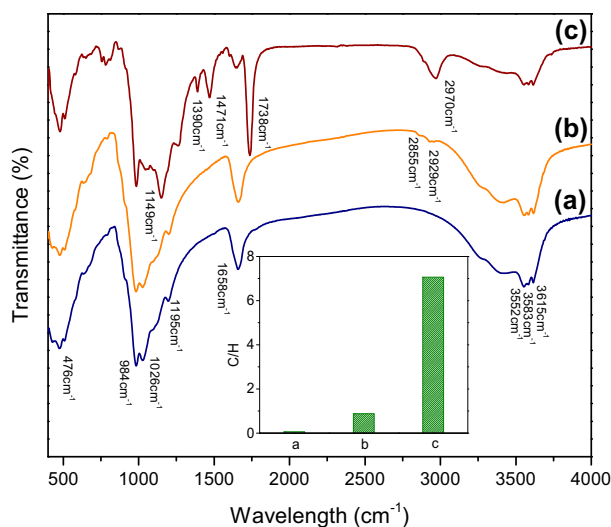


Fig. 3. FT-IR spectra and C/H content ratio of (a) purified palygorskite, (b) silylated palygorskite and (c) SMIP.

vibration for C=C and C=N, confirming the polymerization of functional monomer 4-VP. Apart from this, the characteristic features of the SMIP are C–H bands at 2,970  $\text{cm}^{-1}$  and C–O bands at 1,149  $\text{cm}^{-1}$ . Additionally, the changes in organic content were carried out by elemental analysis of the purified palygorskite, silylated palygorskite, and SMIP as well (Fig. 3). As can be seen from Fig. 3, after silylation treatment, C/H content ratio increased from 0.06 to 0.88, suggesting successful introduction of silane coupling agent onto the surface of the purified palygorskite. After polymerization reaction, the C/H content ratio rose to 7.06. These results provided a clear evidence for the grafting of the MIP to the surface of palygorskite.

### 3.2. Kinetics studies

The adsorption kinetic processes of BPA on the SMIP and MIP were investigated by varying the contact time from 0 to 240 min. As shown in Fig. 4(a), the SMIP offered a faster adsorption dynamics for BPA molecules and more than 90% of the removal efficiency took place within the first 2 min. This fast dynamics adsorption might originate from the high ratio of accessible surface-imprinted sites and the improved binding rate between BPA molecules and recognition sites. Therefore, the BPA templates can be easily enriched on the surface of the SMIP in such a short time. To examine the controlling mechanism of adsorption processes and evaluate the performance of the adsorbents used for BPA adsorption, the pseudo-second-order kinetics and the intra-particle diffusion models were employed to

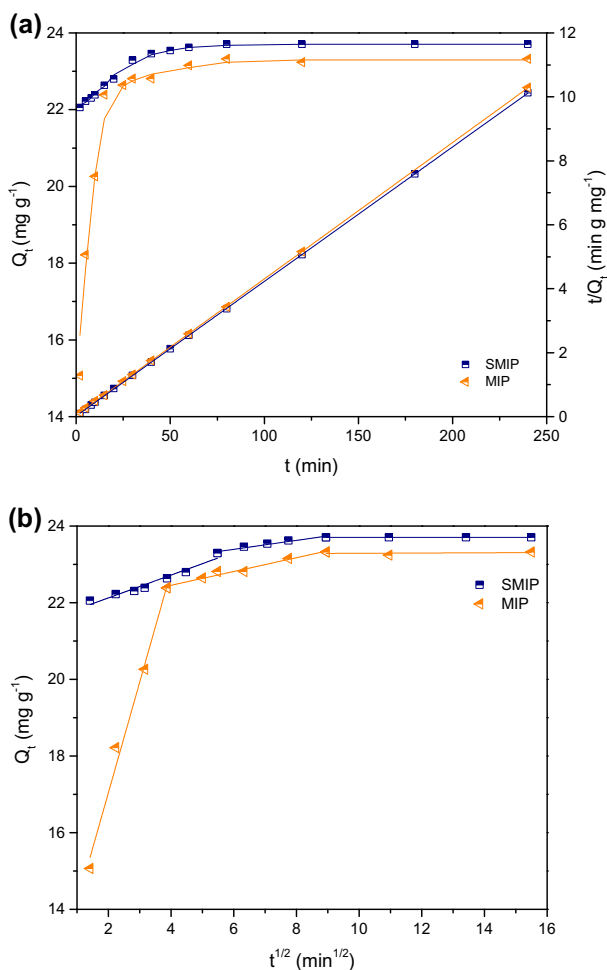


Fig. 4. Adsorption kinetics of the SMIP and MIP for BPA at 298 K: (a) pseudo-second-order and (b) intra-particle diffusion.

analyze the experimental data and their linear forms can be expressed as follows:

$$\frac{t}{Q_t} = \frac{1}{k_2 Q_e^2} + \frac{t}{Q_e} \quad (5)$$

$$Q_t = k_p t^{0.5} + C \quad (6)$$

where  $Q_t$  (mg g<sup>-1</sup>) is the adsorption amount of BPA adsorbed at time  $t$  (min);  $k_2$  (g mg<sup>-1</sup> min<sup>-1</sup>) is the pseudo-second-order rate constant;  $k_p$  (mg g<sup>-1</sup> min<sup>-1/2</sup>) is the intra-particle diffusion rate constant, which is proportional to the boundary layer thickness; and  $C$  is a constant. Moreover, for the pseudo-second-order kinetic model, the initial adsorption rate,  $h$  (mg g<sup>-1</sup> min<sup>-1</sup>), is given by the following equation:

$$h = k_2 Q_e^2 \quad (7)$$

The adsorption rate constants and linear regression correlation coefficients ( $r^2$ ) are summarized in Table 1. Obviously, the adsorption amount of the SMIP for BPA was higher than the MIP. The adsorption of BPA onto SMIP and MIP followed pseudo-second-order kinetics according to the favorable fit between experimental and calculated values of  $Q_e$  (all  $r^2$  values above 0.99), which is also shown in Fig. 4(a). And it was assumed that chemical process could be the rate-limiting step in the adsorption process for BPA, which was consistent with the formation of non-covalent bonds between BPA template molecules and functional monomer during the preparation of imprinted polymers. Moreover, multi-linearity in the shape of the intra-particle diffusion plot (Fig. 4(b)) indicated that three steps were involved in the process of BPA adsorption. The initial stage was attributed to the diffusion of BPA through film diffusion to the outer surface of adsorbents. The second stage described the gradual adsorption stage, during which both film diffusion and intra-particle diffusion were simultaneously operating. The last stage was the final equilibrium stage where the intra-particle diffusion started to slow down due to extremely low concentration of BPA left in solution. It was also found that the initial adsorption rate ( $h$ ) of the SMIP was more than double that of the MIP, which may lie in the formation of surface-exposed and specific recognition cavities on the palygorskite supports during the imprinting reaction, which benefited for BPA to diffuse into the inner cavities of the polymer. As for the MIP, the stiff polymer network, however, prevents efficient removal of the template from the interior of the MIP, resulting in slow binding kinetics. In addition, it is necessary to note that the intercept  $C$  as proposed by Eq. (6) was not zero but a large value, indicating that intra-particle diffusion may not be the controlling factor in determining the kinetics of the BPA adsorption process.

### 3.3. Adsorption isotherms

The adsorption amounts of BPA bound to the SMIP and MIP as a function of residual BPA concentration in solution are presented in Fig. 5. It was noted that the adsorption amount of both adsorbents increased with increasing BPA equilibrium concentration, while, the adsorption capacity of the SMIP for BPA was superior to that of the MIP, which was ascribable to the combination of more exposed imprinted cavities and large surface area provided by

Table 1

Kinetic parameters of the pseudo-second-order and intra-particle diffusion equation for BPA adsorption onto the SMIP and MIP

Sample	Pseudo-second-order				Intra-particle diffusion		
	$Q_e$ (mg g <sup>-1</sup> )	$k_2$ (g mg <sup>-1</sup> min <sup>-1</sup> )	$h$ (mg g <sup>-1</sup> min <sup>-1</sup> )	$r^2$	$k_p$ (mg g <sup>-1</sup> min <sup>-1/2</sup> )	$C$	$r^2$
SMIP	23.769	0.085	48.123	0.999	0.130	22.217	0.714
MIP	23.447	0.042	23.111	0.999	0.438	18.758	0.405

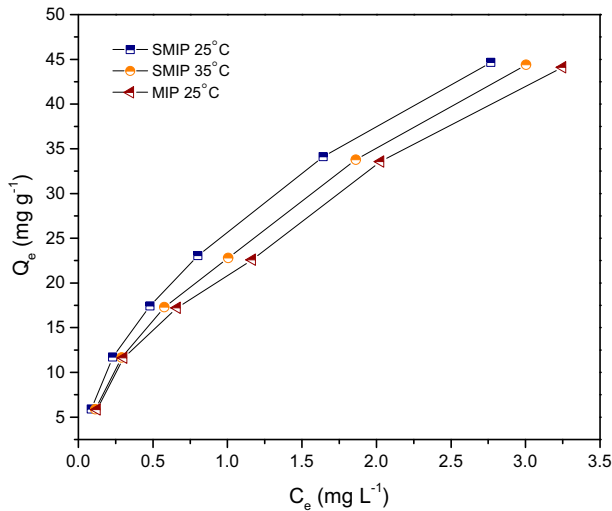


Fig. 5. Adsorption isotherm for BPA adsorption onto SMIP and MIP.

palygorskite support. Furthermore, the observed decrease in the adsorption amount with an increase of temperature was indicative of the exothermic nature of adsorption process. To further study the adsorption mechanism, the Langmuir, Freundlich, and Dubinin–Radushkevich isotherm models were applied to estimate the adsorption behavior of the non-covalently imprinting adsorbents, which can be described by Eqs. (8)–(10), respectively:

$$\frac{1}{Q_e} = \frac{1}{Q_m} + \frac{1}{bQ_m C_e} \quad (8)$$

$$\ln Q_e = \ln K_F + \frac{\ln C_e}{n} \quad (9)$$

$$\ln Q_e = \ln Q_m - \beta \varepsilon^2, \varepsilon = RT \ln \left( 1 + \frac{1}{C_e} \right) \quad (10)$$

where  $Q_m$  (mg g<sup>-1</sup>) represents monolayer adsorption capacity;  $b$  (L mg<sup>-1</sup>) is the affinity constant;  $K_F$  (mg g<sup>-1</sup>) and  $1/n$  (dimensionless) are the Freundlich constants for the adsorption capacity and heterogeneity factor of

the adsorbent, respectively;  $\varepsilon$  is the Polanyi potential;  $R$  (8.314 J mol K<sup>-1</sup>) is the gas constant;  $T$  (K) is the absolute temperature; and  $\beta$  (mol<sup>2</sup> kJ<sup>-2</sup>) is the activity coefficient related to mean adsorption energy ( $E$ , kJ mol<sup>-1</sup>), which was defined as the free energy change when per molecule of the adsorbate is transferred to the surface of the solid from infinity in solution, can be calculated by Eq. (11):

$$E = (2\beta)^{-0.5} \quad (11)$$

The corresponding isotherm parameters obtained from the linear analysis are listed in Table 2. The correlation coefficient ( $r^2$ ) revealed that the Freundlich isotherm yielded a better fit than that of Langmuir model isotherm, implying adsorption took place at heterogeneous adsorption sites on the both adsorbent surface. This was perfectly in accordance with the non-linearity ( $0 < 1/n < 1$ ) of all the isotherms. Furthermore, the affinity constant ( $b$ ) and the Freundlich constants ( $K_F$ ) for BPA on the SMIP were higher than those on the MIP, indicating the stronger affinity of the SMIP for BPA. Although the adsorption process did not conform to the D–R isotherm, the  $E$  value of BPA adsorption was in the range of 2.877–3.249 kJ mol<sup>-1</sup>, suggesting the adsorption process may be mainly dependent on hydrogen bonding formed by BPA and functional monomer.

In order to further evaluate the specificity, the Scatchard model was also utilized to fit the experimental data, which can be described as Eq. (12):

$$\frac{Q_e}{C_e} = \frac{Q_{\max} - Q_e}{K_d} \quad (12)$$

where  $Q_{\max}$  (mg g<sup>-1</sup>) is the maximum binding amount. As can be seen from Fig. 6, the Scatchard plot for SMIP and MIP generally consist of two linear sections with different slopes, indicating that there were two classes of binding sites in the SMIP and MIP, and the binding site configuration in both adsorbents is heterogeneous.

Table 2

Langmuir, Freundlich, and D-R isotherm parameters for BPA adsorption onto SMIP and MIP

Sample	T	Langmuir			Freundlich			D-R			
		$Q_m$ ( $\text{mg g}^{-1}$ )	$b$ ( $\text{L mg}^{-1}$ )	$r^2$	$K_F$ ( $\text{mg g}^{-1}$ )	$n$	$r^2$	$Q_m$ ( $\text{mg g}^{-1}$ )	$\beta$ ( $\text{mol}^2 \text{kJ}^{-2}$ )	$E$ ( $\text{kJ mol}^{-1}$ )	$r^2$
SMIP	298	40.306	1.929	0.989	25.758	1.730	0.995	32.450	0.047	3.249	0.870
	308	42.141	1.409	0.990	23.231	1.649	0.996	31.733	0.053	3.058	0.856
MIP	298	41.545	1.312	0.990	21.762	1.664	0.993	31.099	0.060	2.877	0.849

### 3.4. Adsorption selectivity

In order to evaluate the selectivity of the SMIP and MIP, experiments studying competitive adsorption of BPA and its structural analogs, (i.e. 4-TBP and HQ) from their mixtures were conducted under the same conditions. The area percentage of adsorption peak corresponding to the competitive target compounds are depicted in Fig. 7. It has been found that both adsorbents exhibit a much higher adsorption amount towards the BPA template molecules than the other analogs, particularly for SMIP. The difference in the selective recognition ability for BPA between SMIP and MIP is more specifically reflected in Table 3. For the higher values of the adsorption amount, distribution coefficient  $K_d$  of the SMIP could be attributed to more specific binding sites in the imprinted layer on palygorskite surface imparted by precipitation polymerization reaction. Meanwhile, the  $k$  values of SMIP for 4-TBP and HQ were 2.05 and 1.41 times greater than MIP, respectively. All of these results provided

clear evidence of the good binding selectivity of SMIP in the presence of competitive adsorption molecules.

### 3.5. Regeneration and reuse

The stability and reusability of the SMIP after each recycle was evaluated by regeneration experiments. The spent SMIP was recovered upon treatment with methanol/acetic acid (9/1, v/v) and methanol to elute the adsorbed BPA, and then reused in subsequent cycle. Fig. 8 shows the removal efficiencies of the SMIP for BPA in four adsorption/desorption cycles. It can be seen that the SMIP only lost about 3% of its affinity in the process of four cycles, which is probably caused by the loss of memory cavities during the regeneration process. This value is smaller than that of other MIPs based on kaolinite/ $\text{Fe}_3\text{O}_4$  composites and multi-walled carbon nanotubes [26,27], to some extent, indicating the stable regeneration performance and inherent reusability of the SMIP.

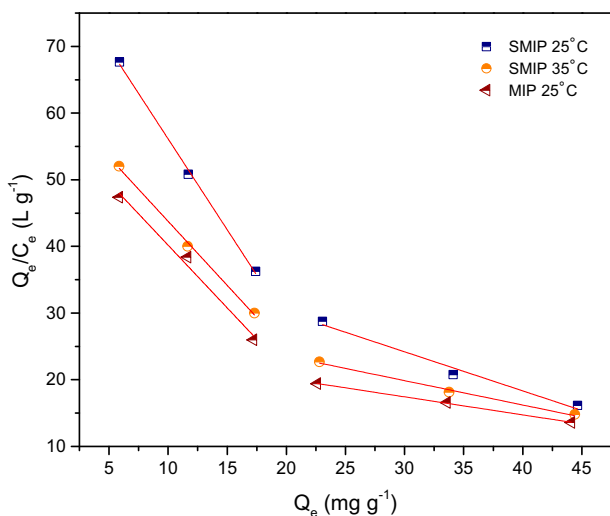


Fig. 6. Scatchard plots of the SMIP and MIP.

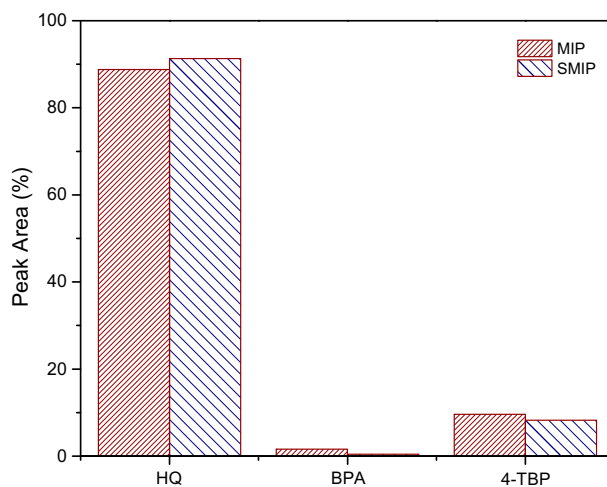


Fig. 7. The area percentage of absorption peak obtained from HPLC.

Table 3  
Distribution coefficient and selectivity coefficient data

Analytes	$Q_e$ (mg g <sup>-1</sup> )		$K_d$ (L g <sup>-1</sup> )		$k$	
	SMIP	MIP	SMIP	MIP	SMIP	MIP
BPA	5.944	5.895	128.390	67.293	–	–
4-TBP	5.180	5.228	7.585	8.131	16.927	8.276
HQ	0.384	0.288	0.082	0.061	1,564.749	1,112.206

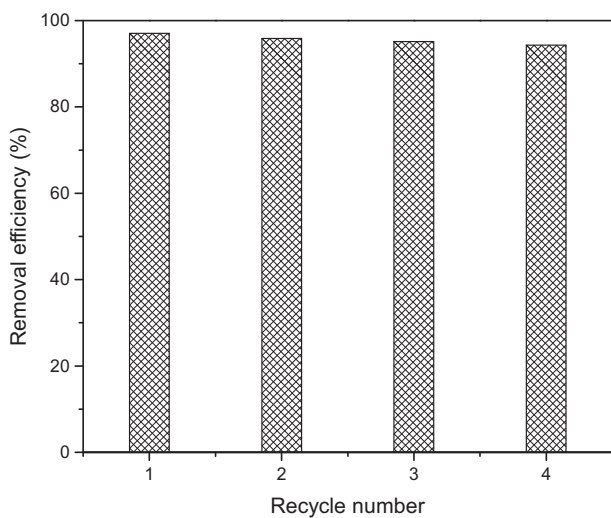


Fig. 8. Regeneration and reuse of the SMIP. Adsorbents dose: 5 mg; initial BPA concentration: 5 mg L<sup>-1</sup>; solution volume: 6 mL; contact time: 2 h.

#### 4. Conclusions

In summary, palygorskite-supported SMIP for BPA template was synthesized and well characterized by SEM, FT-IR and elemental analysis. Compared with its corresponding MIP, the as-prepared SMIP adsorbent, combining the advantages of palygorskite and molecular imprinting technique, possessed outstanding affinity, high efficiency and excellent selectivity towards BPA in aqueous solution. The stable regeneration performance and inherent reusability made the synthesized SMIP attractive for separation and specific recognition. It should be pointed out that even though the preparation process was relatively complex, the palygorskite-supported imprinting approach provided a feasible solution to the removal of BPA in environmental water.

#### Acknowledgment

This work was financially supported by Priority Academic Program Development of Jiangsu Higher

Education Institutions (No. 1105007001), Research Fund for Taihu Lake Pollution Control of Jiangsu Province (No. TH2012207), and Research and Innovation Project for College Graduates of Jiangsu Province (No. CXLX110129).

#### References

- [1] T. Geens, L. Roosens, H. Neels, A. Covaci, Assessment of human exposure to Bisphenol-A, Triclosan and Tetrabromobisphenol-A through indoor dust intake in Belgium, *Chemosphere* 76 (2009) 755–760.
- [2] H. Fromme, T. Kuchler, T. Otto, K. Pilz, J. Müller, A. Wenzel, Occurrence of phthalates and bisphenol A and F in the environment, *Water Res.* 36 (2002) 1429–1438.
- [3] A. Schecter, N. Malik, D. Haffner, S. Smith, T.R. Harris, O. Paepke, L. Birnbaum, Bisphenol A (BPA) in U.S. Food, *Environ. Sci. Technol.* 44 (2010) 9425–9430.
- [4] Y.Q. Huang, C.K.C. Wong, J.S. Zheng, H. Bouwman, R. Barra, B. Wahlström, L. Neretin, M.H. Wong, Bisphenol A (BPA) in China: A review of sources, environmental levels, and potential human health impacts, *Environ. Int.* 42 (2012) 91–99.
- [5] C. Liao, K. Kannan, Widespread occurrence of Bisphenol A in paper and paper products: Implications for human exposure, *Environ. Sci. Technol.* 45 (2011) 9372–9379.
- [6] V. Migeot, A. Dupuis, A. Carriot, M. Albouy-Llaty, F. Pierre, S. Rabouan, Bisphenol A and its chlorinated derivatives in human colostrum, *Environ. Sci. Technol.* 47 (2013) 13791–13797.
- [7] J.R. Rochester, Bisphenol A and human health: A review of the literature, *Reprod. Toxicol.* 42 (2013) 132–155.
- [8] Z. Zhang, J. Hu, Selective removal of estrogenic compounds by molecular imprinted polymer (MIP), *Water Res.* 42 (2008) 4101–4108.
- [9] L. Zhang, J. Lv, T. Xu, L. Yang, X. Jiang, Q. Li, High efficiency removal and recovery of an endocrine disrupting compound–bisphenol AF from wastewaters, *Sep. Purif. Technol.* 116 (2013) 145–153.
- [10] L.K. Boateng, J. Heo, J.R.V. Flora, Y. Park, Y. Yoon, Molecular level simulation of the adsorption of bisphenol A and 17 $\alpha$ -ethinyl estradiol onto carbon nanomaterials, *Sep. Purif. Technol.* 116 (2013) 471–478.
- [11] K. Inumaru, J. Kiyoto, S. Yamanaka, Molecular selective adsorption of nonylphenol in aqueous solution by organo-functionalized mesoporous silica, *Chem. Commun.* (2000) 903–904.

- [12] K. Liu, J. Wei, X. Zhou, N. Liu, Construction of amphiphilic segments on polypropylene nonwoven-surface and its application in removal of endocrine disrupting compounds (EDCs) from aqueous solution, *Appl. Clay Sci.* 337 (2015) 178–187.
- [13] Z. Meng, W. Chen, A. Mulchandani, Removal of estrogenic pollutants from contaminated water using molecularly imprinted polymers, *Environ. Sci. Technol.* 39 (2005) 8958–8962.
- [14] L. Chen, S. Xu, J. Li, Recent advances in molecular imprinting technology: Current status, challenges and highlighted applications, *Chem. Soc. Rev.* 40 (2011) 2922–2942.
- [15] Y. Zhang, J. Zhang, C. Dai, X. Zhou, S. Liu, Sorption of carbamazepine from water by magnetic molecularly imprinted polymers based on chitosan-Fe<sub>3</sub>O<sub>4</sub>, *Carbohydr. Polym.* 97 (2013) 809–816.
- [16] W. Liu, X. Liu, Y. Yang, Y. Zhang, B. Xu, Selective removal of benzothiophene and dibenzothiophene from gasoline using double-template molecularly imprinted polymers on the surface of carbon microspheres, *Fuel* 117 (2014) 184–190.
- [17] W. Zhao, N. Sheng, R. Zhu, F. Wei, Z. Cai, M. Zhai, S. Du, Q. Hu, Preparation of dummy template imprinted polymers at surface of silica microparticles for the selective extraction of trace bisphenol A from water samples, *J. Hazard. Mater.* 179 (2010) 223–229.
- [18] D. Gao, Z. Zhang, M. Wu, C. Xie, G. Guan, D. Wang, A surface functional monomer-directing strategy for highly dense imprinting of TNT at surface of silica nanoparticles, *J. Am. Chem. Soc.* 129 (2007) 7859–7866.
- [19] C. Xie, Z. Zhang, D. Wang, G. Guan, D. Gao, J. Liu, Surface molecular self-assembly strategy for TNT imprinting of polymer nanowire/nanotube arrays, *Anal. Chem.* 78 (2006) 8339–8346.
- [20] H. Wang, Y. He, T. Ji, X. Yan, Surface molecular imprinting on Mn-doped ZnS quantum dots for room-temperature phosphorescence optosensing of pentachlorophenol in water, *Anal. Chem.* 81 (2009) 1615–1621.
- [21] P. Chang, Z. Li, T. Yu, S. Munkhbayer, T. Kuo, Y. Hung, J. Jean, K. Lin, Sorptive removal of tetracycline from water by palygorskite, *J. Hazard. Mater.* 165 (2009) 148–155.
- [22] R.L. Frost, Y. Xi, H. He, Synthesis, characterization of palygorskite supported zero-valent iron and its application for methylene blue adsorption, *J. Colloid Interface Sci.* 341 (2010) 153–161.
- [23] N. Frini-Srasra, E. Srasra, Acid treatment of south Tunisian palygorskite: Removal of Cd(II) from aqueous and phosphoric acid solutions, *Desalination* 250 (2010) 26–34.
- [24] H. Chen, A. Zhong, J. Wu, J. Zhao, H. Yan, Adsorption behaviors and mechanisms of methyl orange on heat-treated palygorskite clays, *Ind. Eng. Chem. Res.* 51 (2012) 14026–14036.
- [25] Y. Kong, J. Yuan, Z. Wang, S. Yao, Z. Chen, Application of expanded graphite/attapulgitite composite materials as electrode for treatment of textile wastewater, *Appl. Clay Sci.* 46 (2009) 358–362.
- [26] Z. Zhang, X. Chen, W. Rao, H. Chen, R. Cai, Synthesis and properties of magnetic molecularly imprinted polymers based on multiwalled carbon nanotubes for magnetic extraction of bisphenol A from water, *J. Chromatogr. B* 965 (2014) 190–196.
- [27] W. Guo, W. Hu, J. Pan, H. Zhou, W. Guan, X. Wang, J. Dai, L. Xu, Selective adsorption and separation of BPA from aqueous solution using novel molecularly imprinted polymers based on kaolinite/Fe<sub>3</sub>O<sub>4</sub> composites, *Chem. Eng. J.* 171 (2011) 603–611.